Eur. Phys. J. D **24**, 49–52 (2003)
DOI: 10.1140/epjd/e2003-00118-5

THE EUROPEAN PHYSICAL JOURNAL D

Magnetic field dependence of electronic structures in a single and double quantum dots by 3D-MHFKS calculation

T. Matsuse[a] and T. Takizawa

Faculty of Textile Science and Technology, Shinshu University, Ueda, Nagano 386-8567, Japan

Received 10 September 2002
Published online 3 July 2003 –

Abstract. The 3-dimensional Mesh-Hartree-Fock-Kohn-Sham (3D-MHFKS) calculation is applied to study the magnetic (B-) field dependence of the electronic structures of circular-shaped vertical quantum dot (Q-dot) with electron number (N) in double barrier structure (DBS) and also coupled double Q-dots in triple barrier structure (TBS). One of the advantageous points of the 3D-MHFKS calculation is that the strength of coupling between two dots are explicitly evaluated by introducing the realistic barrier in TBS as a straightforward extension of 3D-MHFKS calculation of the single Q-dot in DBS. The calculated chemical potentials represented in B–N phase diagram are consistently and systematically discussed by showing the B-field dependence of the occupied single particle energy levels from the view point how the electronic states transfer sequentially from Fock-Darwin (FD) to lowest Landau (LL) and from LL to the spin flip (SF) and from SF to spin-polarized maximum density droplet (MDD) domains as increasing B-field in the Q-dots.

PACS. 73.20.-r Electron states at surfaces and interfaces

1 Introduction

The electronic properties of well-defined circular-shaped vertical Q-dot in DBS [1,2] and coupled double Q-dots in TBS [3,4] have been extensively studied from the viewpoint of artificial atom and molecule, respectively. Especially, the characteristic phase transition measured in the B–N phase diagram indicates the richness of the electronic structures in the Q-dots as have been discussed in the theoretical works with Hartree-Fock method [5] and density functional method [6].

To investigate the B-field induced various transitions of the electronic states measured in single dot in DBS [2] as well as coupled double Q-dots in TBS [4], the introduction of the vertical degree of freedom (3D-effect) is indispensable in the theoretical study to obtain the consistent understanding for the electronic states in the Q-dots.

In the previous work [7], we have presented the framework of the 3D-MHKS-calculation and applied to the studies of the electronic structures in DBS and also TBS. In the TBS, it has been pointed out that the calculated chemical potentials reproduce well the characteristics in the measured B–N phase diagram for the case of weakly coupled double Q-dots which has the pairwise sequences coming from the spin-degeneracy character [3].

In this paper, we apply the 3D-MHFKS calculation to the strongly coupled double Q-dots as well as single dot in the wide range of B-field up to 10 T.

[a] e-mail: tmatsu1@giptc.shinshu-u.ac.jp

2 3D-MHFKS calculation for Q-dots

To investigate the electronic structures in Q-dots of N-electron, we adopt the energy functional E_{HFKS} [8] formulated by Kohn and Sham [9] which is composed of Hartree-Fock energy E_{HF} and correlation energy $E_c[\rho^\alpha, \rho^\beta]$. In this study, we use the local spin density functional presented by Vosko and Wilk [10] for the correlation energy.

To linearize the original HFKS-equation obtained by the variation of the HFKS-energy functional, firstly we introduce the following Coulomb potential $U_{ij}^\sigma(\mathbf{r})$ in local form

$$U_{ij}^\sigma(\mathbf{r}) = \int \frac{1}{|\mathbf{r}-\mathbf{r}'|}\rho_{ij}^\sigma(\mathbf{r}')\mathrm{d}\mathbf{r}' \tag{1}$$

which depends explicitly the single particle wave functions $\psi_i^\sigma(\mathbf{r})$ and densities $\rho_{ij}^\sigma(\mathbf{r}) = \psi_j^{\sigma *}(\mathbf{r})\psi_i^\sigma(\mathbf{r})$, then we can represent the original HFKS equation in local form [11]

$$[h(\mathbf{r}) + U_H(\mathbf{r})]\psi_i^\sigma(\mathbf{r}) - \sum_{j=1}^{N_\sigma} U_{ij}^\sigma(\mathbf{r})\psi_j^\sigma(\mathbf{r}) + v_c^\sigma([\rho^\alpha, \rho^\beta], \mathbf{r})\psi_i^\sigma(\mathbf{r}) = \epsilon_i^\sigma \psi_i^\sigma(\mathbf{r}) \tag{2}$$

Here $h(\mathbf{r})$ denotes a one-body part of the system and $U_H(\mathbf{r})$ the Hartree term.The fourth one $v_c^\sigma([\rho^\alpha, \rho^\beta], \mathbf{r})$ shows the spin-dependent local correlation potential.

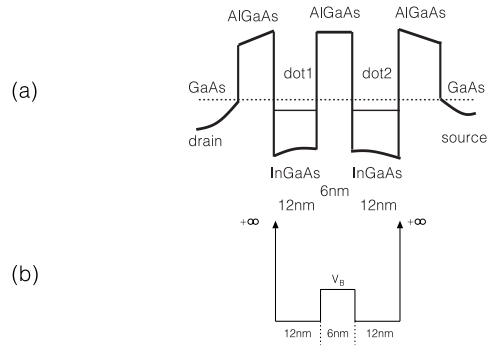

Fig. 1. Schematic presentation of model potential in vertical direction for strongly coupled double dots in TBS. (a) Experimental profile of TBS [3], (b) model potential $U_Z(z)$ in the vertical direction, $V_B = 100$ meV.

When this correlation potential is switched off, equation (2) becomes to be equivalent with the UHF one.

To obtain the self-consistent solution of the local form HFKS-equation (2) in 3-D real space mesh method, we use the Car-Parrinello-like relaxation method and the Coulomb potentials (1) are obtained by solving the Poisson equation $\nabla^2_{\mathbf{r}} U^{\sigma}_{ij}(\mathbf{r}) = -4\pi\rho^{\sigma}_{ij}(\mathbf{r})$ under the proper boundary conditions. To calculate the kinetic energy in this 3D-mesh calculation, the finite difference is applied by using the 9-points in the x and y variables and 7-points for z variable.

For investigating the electronic structure of Q-dots of N-electrons including 3-dimensional effect, we use the total Hamiltonian $\hat{H}_N$ for HF-part

$$\hat{H}_N = \sum_{i=1}^{N} \hat{H}_{XY}(x_i, y_i) + \frac{1}{2}\sum_{i}^{N}\sum_{j}^{N}{}_{i\neq j} \frac{e^2}{\epsilon|\mathbf{r}_i - \mathbf{r}_j|} + \sum_{i=1}^{N} \hat{H}_Z(z_i)$$

where $\hat{H}_{XY}(x,y) = -\frac{\hbar^2}{2m^*}\nabla^2_{xy} + U_C(x,y) + U_B(x,y)$ is the usual 2-dimensional Hamiltonian. The confinement potential $U_C(x,y) = \frac{1}{2}m^*\omega^2(x^2+y^2)$ is used and the magnetic field effect is represented by $U_B(x,y) = \frac{1}{2}m^*\frac{\omega_c^2}{4}(x^2+y^2) + \frac{\omega_c}{2}\hat{l}_z + g^*\mu_B\frac{\mathbf{B}\cdot\mathbf{S}}{\hbar}$ where $\omega_c = \frac{eB}{m^*c}$ is cyclotron frequency. In this calculation, we use the effective mass $m^* = 0.067$, the effective g-factor $g^* = 0.44$ and the dielectric constant $\epsilon = 12.5$.

The vertical degree of freedom in the Q-dots is introduced in $\hat{H}_Z(z)$ with potential $U_Z(z)$ of square well form; $\hat{H}_Z(z) = -\frac{\hbar^2}{2m^*}\frac{\partial^2}{\partial z^2} + U_Z(z)$. All geometrical factors in $\hat{H}_Z(z)$ are settled to be the almost same scale shown in references [1,2] as is shown schematically in Figure 1 in the case of coupled double dots. In the x and y variables, the 21 mesh points with the mesh spacing of 10 nm is used for the case of the confinement of $\hbar\omega = 4$ meV and this set of mash points are used to the other case of the confinement strength by the use of the scaling relation $\sqrt{\omega}$.

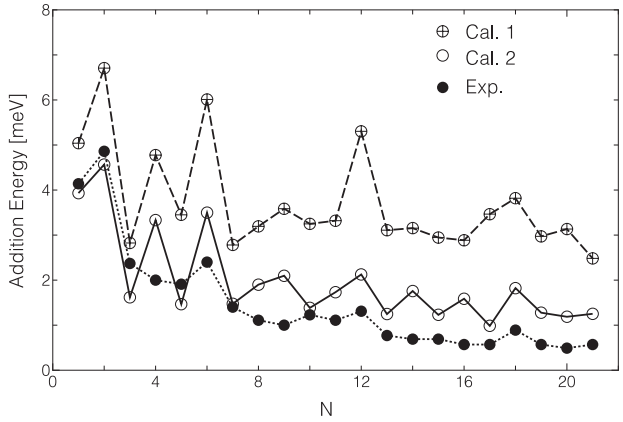

Fig. 2. N-dependence of addition energies of strongly coupled double dots in TBS by 3D-MHFKS calculation and comparison with experimental ones [4] at magnetic field $B = 0$ T. Cal.1 is for the confinement potential of N-independent $\hbar\omega = 5$ meV and Cal.2 for the potential of N-dependent $\hbar\omega_N = \hbar\omega_0 N^{-\frac{1}{4}}$ [13], $\hbar\omega_0 = 5$ meV, respectively.

3 Electronic structures of strongly coupled double Q-dots in TBS

The $U_Z(z)$ potential which determines the coupling between two Q-dots in TBS is shown in Figure 1b by comparing with experimental profile of Figure 1a [3]. As is shown in Figure 1, we use the width 6 nm of the barrier which is the same one of the weakly coupled dots for the convenience of the 3D-mesh in the vertical direction, but the barrier height $V_B = 100$ meV is used to reproduce the coupling energy $\Delta_{\mathrm{SAS}} = 3.4$ meV deduced from the measured one [4].

The addition energies obtained by 3D-MHFKS calculation of the strongly coupled double dots in TBS at magnetic field $B = 0$ T are shown in Figure 2 comparing with the measured ones [4]. In the case of the confinement potential with N-independent $\hbar\omega = 5$ meV, the calculated addition energies are considerably larger than measured ones then we use the N-dependent confinement $\hbar\omega_N = \hbar\omega_0 N^{-\frac{1}{4}}$ [13]. This N-dependent confinement potential of $\hbar\omega_0 = 5$ meV reproduces well in the small electron number region, but in the region larger than $N \simeq 8$, the calculated addition energies are about twice larger than the measured ones.

To exemplify how the effective mean field obtained by the 3D-MHFKS calculation develop with increasing of electron number N, single particle energy levels in TBS obtained by the calculation are shown in Figure 3 in the case of confinement potential of N-independent $\hbar\omega = 5$ meV at magnetic field $B = 0$ T. It can be seen that the 3D-MHFKS calculation has a considerably large effect to weaken the strength of the confinement potential, but it is not enough to reproduce the N-dependent of the effective confinement potential which are expected from the N-dependence of the addition energies (see Fig. 2). From Figure 3, it is also shown how the bond- and anti-bond states in the 3D-MHFKS calculation develop with increasing of electron number N.

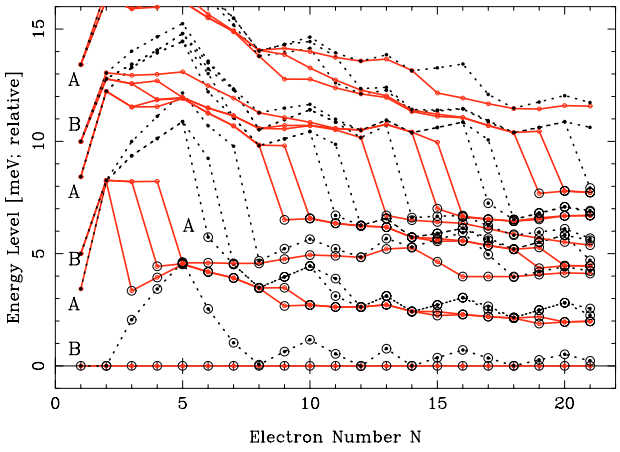

Fig. 3. N-dependence of single particle energy levels of strongly coupled double dots in TBS by 3D-MHFKS calculation for the case of confinement potential of N-independent $\hbar\omega = 5$meV at magnetic field $B = 0$ T. The energy levels are plotted by the differences from the ground state of each electron number N. The open circled levels show the occupied ones. The levels connected with solid lines are for up-spin states and dotted lines for down-spin states. Symbol B shows bond-states and A anti-bond-states.

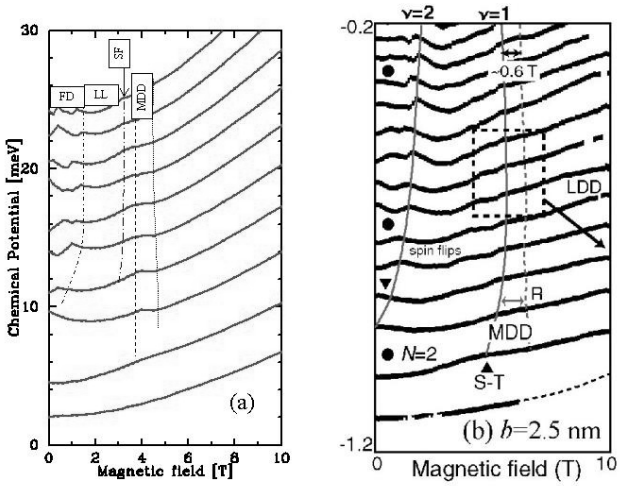

Fig. 4. B–N phase diagrams of strongly coupled double dots in TBS, (a) the obtained chemical potentials by 3D-MHFKS calculation for the confinement potential of N-dependent $\hbar\omega_N = \hbar\omega_0 N^{-\frac{1}{4}}$ [13], $\hbar\omega_0 = 5$ meV and (b) the measured ones [4].

The B-field dependence of the calculated chemical potential of strongly coupled double dots in TBS are shown in Figure 4 up to $N = 10$ and $B = 10$ T by comparing with the measured ones in B–N phase diagram [4]. To make clear the characteristics of the phase transition of the electronic structures depending on the B-field, it is shown in Figure 5 how the occupied single particle energy levels depends on the magnetic field B for the case of $N = 10$.

As can be seen in Figure 5, at the weak B-field region up to $B \simeq 1.5$ T, the occupied states are constructed by the well-known Fock-Darwin (FD) states which are indicated FD in Figure 4. After the last crossing of FD-states and the lowest Landau levels at $B \simeq 1.5$ T, the occupied

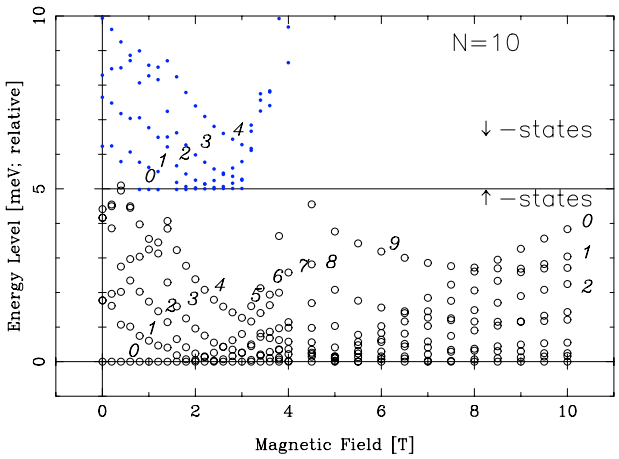

Fig. 5. B-field dependence of the occupied single particle energy levels of strongly coupled double dots in TBS by 3D-MHFKS calculation for the case of electron number $N = 10$ for the confinement potential of N-dependent $\hbar\omega_N = \hbar\omega_0 N^{-\frac{1}{4}}$ [13], $\hbar\omega_0 = 5$ meV. The open circled levels are for the up-spin states and plotted by the differences from the ground states of each magnetic field B. The pointed levels are for the down-spin states and plotted by augmentation of 5 meV for visualisation. The numbers in the figures show the angular momentum of the occupied single particle levels.

states are almost composed of the lowest Landau levels which are occupied with the filling factor $\nu = 2$ up to $B \simeq 3.0$ T as is shown by symbol LL in Figure 4. In the very narrow B-fields region from $B \simeq 3.0$ T to 4.0 T, the spin flip (SF) transitions occur and the filling factor ν decreases very rapidly from 2 to 1 of full spin polarized states. Then all electronic states with full spin-polarization occupied by the lowest Landau levels appear and form the so-called maximum density droplet (MDD) in very narrow region from $B \simeq 4.0$ T to 5.0 T. As the B-fields are increased furthermore, the occupied single particle levels begin to deviate from the normal angular momentum sequence of the lowest Landau levels. In fact the single particle states with the lower angular momentums transfer to the excited states in order then the states with larger angular momentum become to the ground state in sequence. In this 3D-MHFKS calculation, it is not identify whether the deviation from the normal sequence of lowest Landau levels correspond the lower density droplet (LDD) or not.

4 Electronic structures of single dot in DBS

In single Q-dot, it had been verified that the wave functions in the vertical direction are composed of the ground state wave function with almost sine shape and the function weaken considerably the two-body Coulomb energy of the two-dimensional limit.

For reproducing well the N-dependence of the measured addition energies of the single Q-dot in the magnetic field $B = 0$ T up to about $N = 20$ [1], we use the

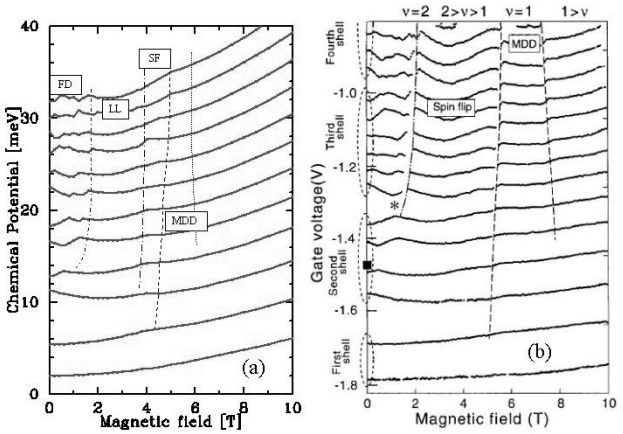

Fig. 6. B–N phase diagrams of single dot in DBS, (a) the obtained chemical potentials by 3D-MHFKS calculation for the confinement potential of N-dependent $\hbar\omega_N = \hbar\omega_0 N^{-\frac{1}{4}}$ [13], $\hbar\omega_0 = 7$ meV and (b) the measured ones [2].

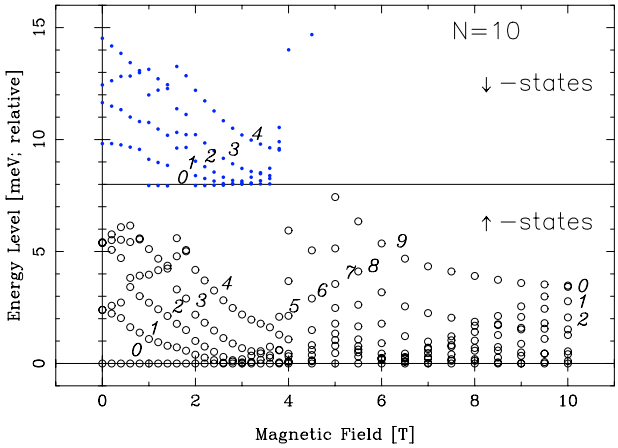

Fig. 7. B-field dependence of the occupied single particle energy levels of single dot in DBS by 3D-MHFKS calculation for the case of electron number $N = 10$ for the confinement potential of N-dependent $\hbar\omega_N = \hbar\omega_0 N^{-\frac{1}{4}}$ [13], $\hbar\omega_0 = 7$ meV. The pointed levels are for the down-spin states and plotted by augmentation of 8 meV for visualisation. For others see the caption of Figure 5.

N-dependent confinement $\hbar\omega_N = \hbar\omega_0 N^{-\frac{1}{4}}$ [13] of $\hbar\omega = 7$ meV in the 3D-MHFKS calculation.

The B-field dependence of the calculated chemical potential in DBS are shown in Figure 6 up to $N = 12$ and $B = 10$ T by comparing with the measured ones in B–N phase diagram [2]. To exemplify the characteristics of the phase transition of the electronic structures depending on the B-field, it is shown how single particle energy levels of single dot in DBS obtained by 3D-MHFKS calculation changes with increasing the magnetic field B for the case of $N = 10$ in Figure 7.

The characteristics differences of electronic structures in between DBS and TBS can be understood by comparing Figure 4 and Figure 6 in B–N phase diagram and also Figure 5 and Figure 7 in the B-dependence of the occupied single particle energy levels. Although all transitions in DBS shift up about 0.5 T to stronger B-field region where the transitions occur in TBS, the 3D-MHFKS calculation obtained the almost similar B–N phase diagrams in both dots in DBS and TBS which correspond well the measured ones [2,4].

5 Conclusion

The 3D-MHFKS calculation are applied to the study of the B-field dependent transition of electronic structures in single dot and strongly coupled double dots and the characteristics of the phase transition are clarified by showing the B-dependence of the occupied single particle levels as shown in Figure 5 and Figure 7.

In weak B-field region, the electronic states have the properties of FD states. Next through the last crossing of FD states to the LL levels as increasing B-field, the electronic states are almost composed of the LL levels with equi-partition of spin states.

The SF transitions occur rapidly in narrow B-field width of about 1T and the electronic states are constructed by the LL levels of completely spin-polarized states to form MDD. As the B-fields are strengthened furthermore, the occupied single particle levels begin to deviate from the normal angular momentum sequences of the LL levels and are expected to form LDD.

We would like to thank S. Tarucha for the courtesy of his permission which we use the figures in Figures 4 and 6. This work was partly supported by Grant-in-Aid for COE Research (10CE2003) by the Ministry of Education, Science, Sports and Culture of Japan.

References

1. S. Tarucha, D.G. Austing, T. Honda, R.J. van der Hage, L.P. Kouwenhoven, Phys. Rev. Lett. **77**, 3613 (1996)
2. S. Tarucha, D.G. Austing, Y. Tokura, W.G. van der Wiel, L.P. Kouwenhoven, Appl. Phys. A **71**, 367 (2000)
3. D.G. Austing, T. Honda, S. Tarucha, Jpn J. Appl. Phys. **36**, 1667 (1997)
4. S. Amaha, D.G. Austing, Y. Tokura, K. Muraki, K. Ono, S. Tarucha, Solid State Comm. **119**, 183 (2001)
5. A.H. MacDonald, S.R.E. Yang, M.D. Johnson, Aust. J. Phys. **46**, 345 (1993)
6. S.M. Reimann, M. Koskinen, M. Manninen, B. Mottelson, Phys. Rev. Lett. **83**, 3270 (1999)
7. T. Matsuse, T. Hama, H. Kaihatsu, N. Toyoda, T. Takizawa, Eur. Phys. J. D **16**, 391 (2001)
8. R.G. Parr, W. Yang, *Density-Functional Theory of Atoms and Molecules* (Oxford University Press, 1989)
9. W. Kohn, L.J. Sham, Phys. Rev. **140**, A1133 (1965)
10. S.H. Vosko, L. Wilk, J. Phys. B **16**, 3687 (1983)
11. T. Matsuse, *Proceedings of the XVII RCNP International Symposium on "Innovative Computational Methods in Nuclear Many-Body Problems"*, edited by H. Horiuchi *et al.* (World Scientific, 1998), p. 369
12. R. Car, M. Parrinello, Phys. Rev. Lett. **25**, 2471 (1985)
13. M. Koskinen, M. Manninen, S.M. Reimann, Phys. Rev. Lett. **79**, 1817 (1997)